IEEE Access
Multidisciplinary | Rapid Review | Open Access Journal

Received 26 October 2022, accepted 4 November 2022, date of publication 9 November 2022, date of current version 14 November 2022.

Digital Object Identifier 10.1109/ACCESS.2022.3220891

RESEARCH ARTICLE

Acquisition of Time and Doppler Shift in WFRFT Encrypted Chaotic Direct Sequence Spread Spectrum System

JIANGYAN HE, GUOGANG YUAN, ZILI CHEN, AND XIJUN GAO
Department of UAV Engineering, Shijiazhuang Campus, Army Engineering University of PLA, Shijiazhuang 050003, China
Corresponding author: Guogang Yuan (18228384858@163.com)

ABSTRACT Weighted fractional Fourier transform encrypted chaotic direct sequence spread spectrum (WFRFT-CD3S) signal is aperiodic and complex Gaussian distributed. The aperiodicity and complex Gaussian distribution are conducive to the covert transmission of information but also make it difficult to acquire the WFRFT-CD3S signal. An acquisition method implemented in two steps is proposed to acquire the Doppler-shifted WFRFT-CD3S signal. First, a bidirectional correlation search method is proposed to align the received signal with the local spreading sequence in the time domain. The correlation peak attenuation caused by the Doppler frequency shift is eliminated by differential. Second, the accumulated phase angle caused by the Doppler frequency shift is obtained by the differential correlation value between the aligned received signal and the local spreading sequence. Then, the Doppler frequency shift is estimated by the accumulated phase angle. The detection probability, the false alarm probability, and the root mean square error (RMSE) of the Doppler shift estimation are analyzed theoretically and simulated. The theoretical results are verified by simulation. Theoretical results and simulations show that the detection probability is higher than 0.999, the false alarm probability is less than 0.001, and the RMSE of Doppler shift estimation is lower than 63 Hz when the signal-to-noise ratio is higher than -7.3 dB.

INDEX TERMS Acquisition, chaotic direct sequence spread spectrum, aperiodicity, Doppler frequency shift, detection probability, false alarm probability, root mean square error.

SYMBOL LIST

b_k	The k-th message bit of the transmitter.
c_k	c_k is the chaotic sequence corresponding to the k-th message bit. The m-th chip of c_k is $c_{k,m}$.
$c_{0,1}$	System initial value.
$c_{k,1}$	Chaotic initial value of c_k.
q	Tent mapping parameter.
x_k	x_k is the WFRFT-chaotic sequence. The m-th chip of x_k is $x_{k,m}$.
N	Spreading factor.
F^α	The α-order WFRFT matrix.
F	Normalized Fourier transform matrix.
$F_{m,n}$	Element in the m-th row and n-th column in F.
ω_m^α	Weighting coefficient of the WFRFT matrix.
P	Inverse matrix.
s_n	Transmitted WFRFT-CD3S signal.
s_k	s_k is the WFRFT-CD3S signal when transmitting b_k. The m-th chip of s_k is $s_{k,m}$.
y_n	Received WFRFT-CD3S signal.
y_k	y_k is the received signal corresponding to s_k. The m-th chip of y_k is $y_{k,m}$.
f_d	Doppler frequency shift.
ϕ_0	Initial phase of received signal.
τ_0	Transmission delay.
T_c	Chip duration.
v_n	White Gaussian noise.
σ^2	Variance of Gaussian white noise.
P_c	Average chip energy.
$G(f_d)$	The correlation value attenuation of the WFRFT-chaotic sequence caused by Doppler frequency.

The associate editor coordinating the review of this manuscript and approving it for publication was Walid Al-Hussaibi.

$\tilde{y}_{k,m}$	$\tilde{y}_{k,m}$ is the differential received signal in the time acquisition process, and the number of chips contained in the delay is N.
$\tilde{x}_{k,m}$	$\tilde{x}_{k,m}$ is the differential WFRFT-chaotic signal in the time acquisition process, and the number of chips contained in the delay is N.
a_{cc}	Acceleration of vehicle.
$G'(a_{\mathrm{cc}})$	The correlation value attenuation of the differential signals caused by vehicle speed variation.
y_a	The received signal segment in the a-th round of correlation search.
$\tilde{y}_a$	The differential received signal in the a-th round of correlation search.
$\tilde{x}_k$	$\tilde{x}_k$ is the differential WFRFT-chaotic sequence in the time acquisition process, and the m-th chip of $\tilde{x}_k$ is $\tilde{x}_{k,m}$.
g_k	Output of the matched filter corresponding to $\tilde{x}_k$.
$\lvert g_{\max}\rvert$	Maximum output magnitude of the three matched filters in Fig. 2.
Z_{T}	Acquisition threshold.
$\hat{\tau}_0$	Estimation of transmission delay.
$d_{k,m}$	Despread signal.
g'	Output of the matched filter in Doppler shift estimation process.
$\hat{f}_{\mathrm{d1}}$	Coarse estimate of the Doppler frequency shift.
f_{d2}	Residual Doppler frequency shift.
$\tilde{y}'_{k,m}$	$\tilde{y}'_{k,m}$ is the differential received signal in the Doppler shift estimation process, and the number of chips contained in the delay is L.
$\tilde{x}'_{k,m}$	$\tilde{x}'_{k,m}$ is the differential WFRFT-chaotic signal in the Doppler shift estimation process, and the number of chips contained in the delay is L.
L	The number of chips contained in the delay of differential processing.
g_{fd}	Correlation value of $\tilde{y}'_{k,m}$ and $\tilde{x}'_{k,m}$.
$\mu_{g_{\mathrm{fd}}}$	Mathematical expectation of g_{fd}.
$\sigma^2_{g_{\mathrm{fd}}}$	Variance of g_{fd}.
θ	Phase angle of g_{fd}.
f_θ	The probability density function of θ.
σ^2_θ	Variance of θ.
$\hat{f}_{\mathrm{d2}}$	Fine estimation of the Doppler frequency shift.
$\hat{f}_{\mathrm{d}}$	The estimation of the Doppler frequency shift.
S_{NR}	Signal-to-noise ratio (SNR).
g_{u}	The correlation value when the received signal and the local WFRFT-chaotic sequence are not aligned.
$u_{g_{\mathrm{u}}}$	Mathematical expectation of g_{u}.
$\sigma^2_{g_{\mathrm{u}}}$	Variance of g_{u}.
η_{u}	Magnitude of g_{u}.
$f_{\eta_{\mathrm{u}}}$	The probability density function of η_{u}.
P_{F}	The false alarm probability.
g_{s}	The correlation value when the received signal is aligned with the local WFRFT-chaotic sequence.
$\mu_{g_{\mathrm{s}}}$	Mathematical expectation of g_{s}.
$\sigma^2_{g_{\mathrm{s}}}$	Variance of g_{s}.
η_{s}	Magnitude of g_{s}.
$f_{\eta_{\mathrm{s}}}$	The probability density function of η_{s}.
P_{D}	The detection probability.
$\varepsilon(L)$	Root mean square error (RMSE) of Doppler shift estimation.
$\lvert x\rvert$	Absolute value of x.
$\arg(x)$	Argument of x.
X^{T}	Transpose of matrix X.
$\bar{X}$	Conjugate of matrix X.
$\odot$	Hadamard product operator.
$\mathrm{E}(x)$	Mathematical expectation of x.

I. INTRODUCTION

The broadcast nature of wireless channels makes legitimate communication signals easy to be intercepted by noncooperative receivers. The chaotic direct sequence spread spectrum (CD3S) communication spreads the message bits through the aperiodic chaotic sequence, which is resistant to the periodicity detection [1], [2], [3]. Since the background noise is usually Gaussian and the chaotic sequence is usually non-Gaussian, the noncooperative receiver can still intercept the CD3S signal by analyzing the statistical characteristics of the received signal [4], [5]. The weighted fractional Fourier transform (WFRFT) can change the statistical distribution of the aperiodic signals into Gaussian distribution [6]. Reference [5] proposed a weighted fractional Fourier transform encrypted chaotic direct sequence spread spectrum (WFRFT-CD3S) system, which makes the transmitted signal aperiodic and complex Gaussian distributed. The WFRFT-CD3S system enables message bits to be transmitted covertly and is suitable for enhancing the security of data links for the unmanned aerial vehicle (UAV). However, in the UAV system, the data link suffers from time-selective fading caused by Doppler frequency shift [7], [8], and the acquisition of WFRFT-CD3S signals in the presence of Doppler frequency shift is a challenging issue. In this paper, we further discuss the acquisition of timing and Doppler frequency shift in the WFRFT-CD3S system based on [5].

The Doppler shift attenuates the correlation between the received signal and the local spreading sequence, thereby increasing the complexity of acquisition [9]. So far, few papers have discussed the acquisition of WFRFT-CD3S signals or similar aperiodic CD3S signals in the presence of Doppler shifts. For the periodic direct sequence spread spectrum (DSSS) signal with Doppler frequency shift, the researchers achieve acquisition through the time-frequency two-dimensional search and focus on improving detection performance or reducing computational complexity through different signal processing methods. The extended replica folding acquisition search technique [10] and the all-phase fast Fourier transform [11] were applied to improve detection performance. The compressed sensing theory [12] and the Doppler frequency estimation algorithms [13], [14] were

applied to reduce the computational complexity. Reference [15] proposed a sparse discrete fractional Fourier transform (SDFrFT) algorithm with low computational complexity to acquire high-dynamic DSSS signals, and the SDFrFT algorithm was optimized in [16].

In the DSSS system, the spreading sequence is a fixed periodic binary pseudo-noise (PN) sequence. Different acquisition methods for DSSS signals are based on the periodicity and binary characteristics of PN sequences, and these acquisition methods essentially implement a time-frequency two-dimensional search. In the WFRFT-CD3S system, the spreading sequence is the aperiodic and complex Gaussian distributed WFRFT-chaotic sequence. The acquisition methods for the DSSS signal are not applicable to the WFRFT-CD3S signal for three reasons. First, each bit of the WFRFT-CD3S signal is spread by different WFRFT-chaotic codes. Even if the Doppler frequency shift is not considered, the aperiodic WFRFT-CD3S signal cannot be acquired by a fixed WFRFT-chaotic sequence when the WFRFT-CD3S signal leads the local WFRFT-chaotic sequence [5], [17]. Second, the computational complexity of the time-frequency two-dimensional search is unacceptable since the WFRFT-chaotic sequence is aperiodic. Third, the phase angle of the complex Gaussian distributed WFRFT-CD3S signal is random, making it difficult to estimate the Doppler shift before the synchronization. A possible acquisition method is to periodically insert a pilot signal into the WFRFT-CD3S signal and achieve the acquisition through the pilot assistance. However, the pilot signal destroys the aperiodicity of the transmitted signal and reduces the anti-interception performance of the transmitted signal. When the pilot signal is detected, the noncooperative receivers can implement targeted jamming on the pilot to disrupt the acquisition [18], [19]. Therefore, this study does not use the pilot signal to assist the acquisition.

In this study, we accomplish the acquisition of time and Doppler shifts in two steps instead of directly implementing a time-frequency two-dimensional search. First, we align the received signal with the local spreading sequence by a one-dimensional correlation search in the time domain. This process is named time acquisition. The correlation search is performed on the differential received signal and the local differential spreading sequence. There is only a fixed phase angle offset between the differential received signal and the local differential spreading sequence, but no Doppler frequency shift [20], which will not cause attenuation of the correlation peak. Inspired by [17], the correlation search is implemented bidirectionally to ensure that the correlation peak can be detected regardless of whether the aperiodic received WFRFT-CD3S signal lags or leads the local spreading sequence. After the time acquisition, we coarsely estimate the Doppler frequency shift by analyzing the spectrum of the despread signal to obtain a relatively large estimation range. Then, the residual Doppler shift is finely estimated by the correlation of the differential received signal and the local differential spreading sequence.

The rest of the paper is organized as follows: Section II presents the system model of WFRFT-CD3S. The proposed acquisition method of time and Doppler shift is discussed in detail in Section III. Section IV theoretically analyzes the detection probability, false alarm probability, and root mean square error (RMSE) of Doppler shift estimation. Section V presents the numerical simulation results. Finally, conclusions are given in Section VI.

II. SYSTEM MODEL

In the WFRFT-CD3S system, the message bit b_k is spread by the WFRFT-chaotic sequence $x_k = \left[x_{k,1}, x_{k,2}, \cdots, x_{k,N}\right]^{\mathrm{T}}$. N is the spreading factor. The aperiodic and complex Gaussian distributed WFRFT-chaotic sequence x_k is generated in two steps. First, generate the chaotic sequence $c_k = \left[c_{k,1}, c_{k,2}, \cdots, c_{k,N}\right]^{\mathrm{T}}$ by two chaotic maps. Then, encrypt the chaotic sequence by WFRFT.

The first chaotic map generates the chaotic initial value $c_{k,1}$ according to the system initial value $c_{0,1}$. In this study, the first chaotic map is the Tent map, which is given by

$$c_{k,1} = \begin{cases} c_{k-1,1}/q, & 0 < c_{k-1,1} \le q, \\ \left(1 - c_{k-1,1}\right)/(1-q), & q < c_{k-1,1} < 1, \end{cases} \tag{1}$$

where $q \in (0, 1)$ is the Tent mapping parameter. The system initial value $c_{0,1}$ needs to meet the initial value condition of the first chaotic map. When the first chaotic map is the Tent map, the system initial value $c_{0,1}$ is in (0, 1). The Tent map can generate different chaotic sequences according to different system initial values in (0, 1), but the characteristics of these chaotic sequences are similar. When the system initial value is not in (0, 1), the Tent map cannot generate chaotic sequences.

The second chaotic map generates the chaotic sequence c_k according to chaotic initial value $c_{k,1}$. In this study, the second chaotic map is the improved Logistic map, which is given by

$$c_{k,m+1} = 1 - 2\left(c_{k,m}\right)^2. \tag{2}$$

The WFRFT-chaotic sequence x_k is obtained by encrypting the chaotic sequence c_k by WFRFT. For the chaotic sequence c_k, the α-order WFRFT is given by [21]

$$\begin{aligned} x_k &= F^{\alpha} c_k \\ &= \left(\omega_0^{\alpha} I + \omega_1^{\alpha} F + \omega_2^{\alpha} P + \omega_3^{\alpha} PF\right) c_k, \end{aligned} \tag{3}$$

where F^{α} is the α-order WFRFT matrix. When $\alpha \in [0.8, 1]$, the real and imaginary parts of x_k are independent and obey the same Gaussian distribution [6]. F is the normalized Fourier transform matrix, and its element in the m-th row and n-th column is given by

$$F_{m,n} = \frac{1}{\sqrt{N}} \exp\left[-\mathrm{j}\frac{2\pi}{N}(m-1)(n-1)\right]. \tag{4}$$

The weighting coefficient ω_m^{α} is given by

$$\omega_m^{\alpha} = \frac{1}{4}\sum_{n=0}^{3} \exp\left[\frac{\mathrm{j}2\pi(\alpha - m)n}{4}\right]. \tag{5}$$

The inverse matrix P is given by

$$P = \begin{bmatrix} 1 & 0 & 0 & \cdots & 0 \\ 0 & 0 & 0 & \cdots & 1 \\ \vdots & \vdots & \vdots & \iddots & \vdots \\ 0 & 0 & 1 & \cdots & 0 \\ 0 & 1 & 0 & \cdots & 0 \end{bmatrix}. \tag{6}$$

The WFRFT-CD3S signal is generated by spreading the message bit b_k through the WFRFT-chaotic sequence x_k. This process can be expressed as

$$s_k = b_k x_k, \tag{7}$$

where $s_k = \left[s_{k,1}, s_{k,2}, \cdots s_{k,N}\right]^{\mathrm{T}}$, $s_{k,m} = s_{kN-N+m}$.

When there is a Doppler frequency shift, the received WFRFT-CD3S signal can be expressed as

$$y_n = s_{n-\tau_0} \exp\left(\mathrm{j}2\pi n f_{\mathrm{d}} T_{\mathrm{c}} + \mathrm{j}\phi_0\right) + v_n, \tag{8}$$

where f_{d} is the Doppler frequency shift, ϕ_0 is the initial phase, T_{c} is the chip duration, τ_0 is the transmission delay, and v_n is the white Gaussian noise. The mean and variance of v_n are 0 and σ^2, respectively.

III. ACQUISITION

A. PROBLEM DESCRIPTION

To facilitate analysis of the effects of Doppler frequency shift, the Doppler frequency shift is temporarily assumed to be constant. When there is a Doppler shift, the correlation value of the WFRFT-chaotic sequence x_k can be calculated as

$$\begin{aligned} &\mathrm{E}\left(\sum_{m=1}^{N} \bar{x}_{k,m} x_{k,m} \mathrm{e}^{\mathrm{j}2\pi m f_{\mathrm{d}} T_{\mathrm{c}} + \mathrm{j}\phi}\right) \\ &= P_{\mathrm{c}} \sum_{m=1}^{N} \mathrm{e}^{\mathrm{j}2\pi m f_{\mathrm{d}} T_{\mathrm{c}} + \mathrm{j}\phi} \\ &= P_{\mathrm{c}} \left[\frac{1 - \mathrm{e}^{\mathrm{j}2\pi f_{\mathrm{d}} T_{\mathrm{c}} N}}{1 - \mathrm{e}^{\mathrm{j}2\pi f_{\mathrm{d}} T_{\mathrm{c}}}} \mathrm{e}^{\mathrm{j}2\pi f_{\mathrm{d}} T_{\mathrm{c}} + \mathrm{j}\phi}\right] \\ &= P_{\mathrm{c}} \left[\frac{\left(\mathrm{e}^{-\mathrm{j}\pi f_{\mathrm{d}} T_{\mathrm{c}} N} - \mathrm{e}^{\mathrm{j}\pi f_{\mathrm{d}} T_{\mathrm{c}} N}\right) \mathrm{e}^{\mathrm{j}\pi f_{\mathrm{d}} T_{\mathrm{c}} N}}{\left(\mathrm{e}^{-\mathrm{j}\pi f_{\mathrm{d}} T_{\mathrm{c}}} - \mathrm{e}^{\mathrm{j}\pi f_{\mathrm{d}} T_{\mathrm{c}}}\right) \mathrm{e}^{\mathrm{j}\pi f_{\mathrm{d}} T_{\mathrm{c}}}} \mathrm{e}^{\mathrm{j}2\pi f_{\mathrm{d}} T_{\mathrm{c}} + \mathrm{j}\phi}\right] \\ &= N P_{\mathrm{c}} \frac{\sin\left(\pi f_{\mathrm{d}} T_{\mathrm{c}} N\right)}{N \sin\left(\pi f_{\mathrm{d}} T_{\mathrm{c}}\right)} \mathrm{e}^{\mathrm{j}\pi f_{\mathrm{d}} T_{\mathrm{c}} (N+1) + \mathrm{j}\phi}, \end{aligned} \tag{9}$$

where the average chip energy P_{c} is given by

$$\begin{aligned} P_{\mathrm{c}} &= \mathrm{E}\left(x_{k,m} \bar{x}_{k,m}\right) \\ &\approx \frac{1}{N} \sum_{m=1}^{N} x_{k,m} \bar{x}_{k,m}. \end{aligned} \tag{10}$$

Equation (9) shows that the Doppler frequency shift f_{d} attenuates the correlation peak of the WFRFT-chaotic sequence x_k by

$$G\left(f_d\right) = \frac{\sin\left(\pi f_{\mathrm{d}} T_{\mathrm{c}} N\right)}{N \sin\left(\pi f_{\mathrm{d}} T_{\mathrm{c}}\right)}. \tag{11}$$

Inspired by [20], we remove the Doppler shift in the received signal by differential processing. The differential received signal is given by

$$\tilde{y}_{k,m} = y_{k,m} \bar{y}_{k-1,m}, \tag{12}$$

where $y_{k,m}$ represents the received signal corresponding to $s_{k,m}$. The WFRFT-chaotic sequence is differentiated accordingly as follows

$$\tilde{x}_{k,m} = x_{k,m} \bar{x}_{k-1,m}. \tag{13}$$

The correlation value between the differential signal $\tilde{x}_{k,m}$ and $\tilde{y}_{k,m}$ is given by

$$\begin{aligned} &\mathrm{E}\left(\sum_{m=1}^{N} \bar{x}_{k,m} x_{k-1,m} y_{k,m} \bar{y}_{k-1,m}\right) \\ &= \mathrm{E}\left[\sum_{m=1}^{N} \bar{x}_{k,m} x_{k-1,m} \left(s_{k,m} \mathrm{e}^{\mathrm{j}2\pi m f_{\mathrm{d}} T_{\mathrm{c}} + \mathrm{j}\phi_k} + v_{k,m}\right)\right. \\ &\quad \left. \cdot \left(\bar{s}_{k-1,m} \mathrm{e}^{-\mathrm{j}2\pi m f_{\mathrm{d}} T_{\mathrm{c}} - \mathrm{j}\phi_{k-1}} + \bar{v}_{k-1,m}\right)\right] \\ &= \mathrm{E}\left(\sum_{m=1}^{N} b_k b_{k-1} \bar{x}_{k,m} x_{k,m} x_{k-1,m} \bar{x}_{k-1,m} \mathrm{e}^{\mathrm{j}2\pi N f_{\mathrm{d}} T_{\mathrm{c}}}\right. \\ &\quad + \bar{x}_{k,m} x_{k-1,m} v_{k,m} \bar{v}_{k-1,m} \\ &\quad + \bar{x}_{k,m} x_{k-1,m} b_k x_{k,m} \mathrm{e}^{\mathrm{j}2\pi m f_{\mathrm{d}} T_{\mathrm{c}} + \mathrm{j}\phi_k} \bar{v}_{k-1,m} \\ &\quad \left. + \bar{x}_{k,m} x_{k-1,m} v_{k,m} b_{k-1} \bar{x}_{k-1,m} \mathrm{e}^{-\mathrm{j}2\pi m f_{\mathrm{d}} T_{\mathrm{c}} - \mathrm{j}\phi_{k-1}}\right) \\ &= \mathrm{E}\left(\sum_{m=1}^{N} b_k b_{k-1} \bar{x}_{k,m} x_{k,m} x_{k-1,m} \bar{x}_{k-1,m} \mathrm{e}^{\mathrm{j}2\pi N f_{\mathrm{d}} T_{\mathrm{c}}}\right) \\ &= N P_{\mathrm{c}}^2 b_k b_{k-1} \mathrm{e}^{\mathrm{j}2\pi N f_{\mathrm{d}} T_{\mathrm{c}}}. \end{aligned} \tag{14}$$

Since there is only a phase offset but no frequency offset between $\tilde{x}_{k,m}$ and $\tilde{y}_{k,m}$, the magnitude of the correlation value in (14) is not attenuated. Furthermore, the phase angle in (14) contains the Doppler shift f_{d}. Therefore, the Doppler shift f_{d} can be estimated from (14) when the received signal is aligned with the local WFRFT-chaotic sequence.

The above analysis assumes that the Doppler frequency shift is constant. However, the Doppler frequency shift varies with vehicle speed in the engineering. Assuming that the vehicle performs a uniformly accelerated motion with the acceleration of a_{cc} when receiving the message bit b_{k-1}, the Doppler frequency corresponding to the m-th chip of b_{k-1} can be expressed as

$$f_{\mathrm{d}}(m) = f_{\mathrm{d}0} + m\Delta f_{\mathrm{d}}, \tag{15}$$

$$\Delta f_{\mathrm{d}} = \frac{a_{\mathrm{cc}} T_{\mathrm{c}}}{\lambda}, \tag{16}$$

where $f_{\mathrm{d}0}$ represents the initial Doppler frequency shift, Δf_{d} represents the Doppler frequency variation between adjacent chips, and λ is the carrier wavelength. When the Doppler

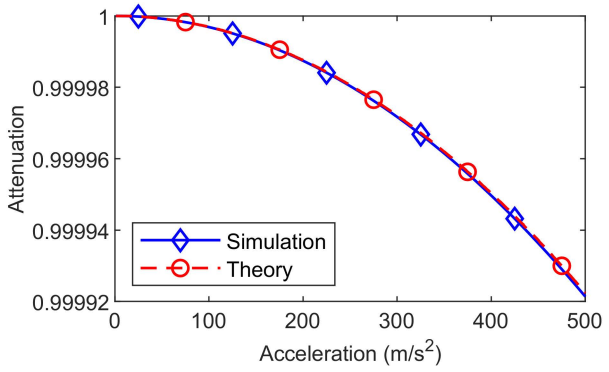

FIGURE 1. Curve of the attenuation of the correlation peak of the differential signals as a function of acceleration.

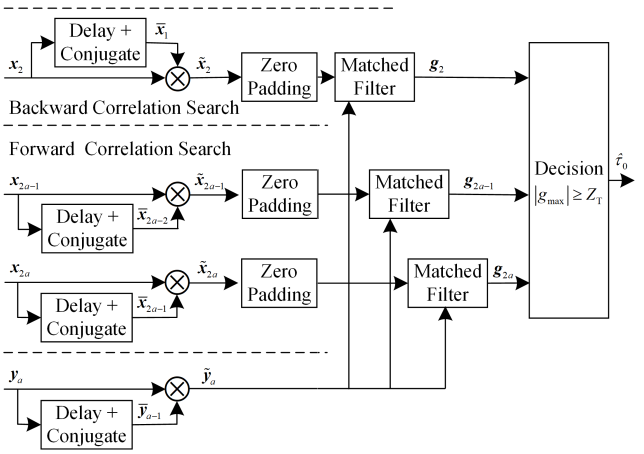

FIGURE 2. Block diagram of time acquisition based on bidirectional correlation search.

frequency shift varies, the correlation value between the differential signal $\tilde{x}_{k,m}$ and $\tilde{y}_{k,m}$ is given by

$$
\begin{aligned}
&\mathrm{E}\left(\sum_{m=1}^{N}\bar{x}_{k,m}x_{k-1,m}y_{k,m}\bar{y}_{k-1,m}\right)\\
&=\mathrm{E}\left[\sum_{m=1}^{N}\bar{x}_{k,m}x_{k-1,m}\left(\bar{s}_{k-1,m}\mathrm{e}^{-\mathrm{j}2\pi m(f_{\mathrm{d}0}+m\Delta f_{\mathrm{d}})T_{\mathrm{c}}-\mathrm{j}\phi_{k-1}}+\bar{v}_{k-1,m}\right)\right.\\
&\quad\left.\cdot\left(s_{k,m}\mathrm{e}^{\mathrm{j}2\pi(m+N)[f_{\mathrm{d}0}+(m+N)\Delta f_{\mathrm{d}}]T_{\mathrm{c}}+\mathrm{j}\phi_{k-1}}+v_{k,m}\right)\right]\\
&=\mathrm{E}\left(\sum_{m=1}^{N}b_kb_{k-1}x_{k-1,m}\bar{x}_{k-1,m}\bar{x}_{k,m}x_{k,m}\mathrm{e}^{\mathrm{j}2\pi(2mN\Delta f_{\mathrm{d}})T_{\mathrm{c}}+\mathrm{j}\Delta\phi}\right.\\
&\quad+\bar{x}_{k,m}x_{k-1,m}\bar{v}_{k-1,m}v_{k,m}\\
&\quad+\bar{x}_{k,m}x_{k-1,m}b_{k-1}\bar{x}_{k-1,m}\mathrm{e}^{-\mathrm{j}2\pi m(f_{\mathrm{d}0}+m\Delta f_{\mathrm{d}})T_{\mathrm{c}}-\mathrm{j}\phi_{k-1}}v_{k,m}\\
&\quad\left.+\bar{x}_{k,m}x_{k-1,m}\bar{v}_{k-1,m}b_kx_{k,m}\mathrm{e}^{\mathrm{j}2\pi(m+N)[f_{\mathrm{d}0}+(m+N)\Delta f_{\mathrm{d}}]T_{\mathrm{c}}+\mathrm{j}\phi_{k-1}}\right)\\
&=\mathrm{E}\left(\sum_{m=1}^{N}b_kb_{k-1}x_{k-1,m}\bar{x}_{k-1,m}\bar{x}_{k,m}x_{k,m}\mathrm{e}^{\mathrm{j}2\pi(2mN\Delta f_{\mathrm{d}})T_{\mathrm{c}}+\mathrm{j}\Delta\phi}\right)\\
&=NP_{\mathrm{c}}^2b_kb_{k-1}\frac{\sin\left(2\pi N^2\Delta f_{\mathrm{d}}T_{\mathrm{c}}\right)}{N\sin\left(2\pi N\Delta f_{\mathrm{d}}T_{\mathrm{c}}\right)}\mathrm{e}^{\mathrm{j}\pi N\Delta f_{\mathrm{d}}T_{\mathrm{c}}(N+1)+\mathrm{j}\Delta\phi},
\end{aligned}
\tag{17}
$$

where $\Delta\phi = Nf_{\mathrm{d}0} + N^2\Delta f_{\mathrm{d}}$.

According to (16) and (17), the acceleration of the vehicle attenuates the correlation peak of the differential signals by

$$
G'(a_{\mathrm{cc}}) = \frac{\sin\left(2\pi a_{\mathrm{cc}}N^2T_{\mathrm{c}}^2\lambda^{-1}\right)}{N\sin\left(2\pi a_{\mathrm{cc}}NT_{\mathrm{c}}^2\lambda^{-1}\right)} \tag{18}
$$

Fig. 1 shows the curve of the attenuation of the correlation peak of the differential signal with the acceleration. In Fig. 1, the carrier frequency is 2 GHz, the carrier wavelength λ is 0.15 m, the spreading factor N is 1000, the chip duration T_{c} is 1 μs, and the initial velocity of the vehicle is 300 m/s. In Fig. 1, the theoretical result in (18) is consistent with the simulation results. When the acceleration is 500 m/s^2, the correlation peak of the differential signals is attenuated by 0.99992. The acceleration of UAV is usually much less than 500 m/s^2. Therefore, the Doppler frequency variation can be ignored in the engineering. Since the Doppler frequency variation has little impact on acquisition performance, the Doppler frequency is assumed to be constant in the remainder of this paper to simplify the analysis.

Based on the above analysis, we acquire the WFRFT-CD3S signal with Doppler shift in two steps. First, align the received signal with the local spreading sequence by a one-dimensional correlation search between $\tilde{x}_{k,m}$ and $\tilde{y}_{k,m}$. Second, estimate the Doppler shift according to (14).

B. TIME ACQUISITION

The WFRFT-chaotic sequence is aperiodic, and the received signal may lag or lead the local WFRFT-chaotic sequence. Therefore, the direction of the correlation search must be consistent with the delay to achieve acquisition. Considering that the delay is unknown, we propose a time acquisition method based on a bidirectional correlation search, which consists of a forward correlation search channel and a backward correlation search channel.

During the correlation search, the unknown binary message bits limit the coherent integration time. In order to avoid the phase inversion, the correlation search must be performed through the WFRFT-chaotic sequence x_k corresponding to the single message bit b_k. In [17], the received signal is also divided into segments of N chips to facilitate parallel search. However, this approach results in that the number of aligned chips falls between $N/2$ and N when detection happens, thereby reducing the detection probability. In this study, to ensure that the number of aligned chips is always N, we divide the received signal into segments with a length of $2N$ chips and N chips overlap.

The proposed time acquisition method based on bidirectional correlation search is shown in Fig. 2. In order to avoid the attenuation of the correlation peak due to Doppler

shift, the received signal and the local WFRFT-chaotic sequence are differentiated. Correlation search is performed by matched filters. Each matched filter performs one round of correlation search every time N chips of y_n are received. a represents the rounds of correlation search.

In Fig. 2, the received signal segment y_a and the differential received signal $\tilde{y}_a$ are given by

$$y_a = [y_{aN-N+1}, y_{aN-N+2}, \cdots, y_{aN+N}]^{\mathrm{T}}, \tag{19}$$

$$\tilde{y}_a = y_a \odot \bar{y}_{a-1}, \tag{20}$$

The local WFRFT-chaotic sequence x_k still contains only N chips. The differential WFRFT-chaotic sequence $\tilde{x}_k$ is given by

$$\tilde{x}_k = x_k \odot \bar{x}_{k-1}. \tag{21}$$

To make the two input sequences of the matched filter equal in length, the differential WFRFT-chaotic sequence is zero-padded to $2N$ chips. The output of the matched filter is given by

$$g_k = F^{-1}\left[\left(F\tilde{y}_a\right) \odot \left(\overline{FU_N\tilde{x}_k}\right)\right], \tag{22}$$

where F^{-1} is the inverse Fourier transform matrix, $U_N = \left[I_N, O_{N,N}\right]^{\mathrm{T}}$ is the zero padding matrix, I_N is the N-order identity matrix, and $O_{N,N}$ is the $N \times N$ zero matrix.

In the backward search channel, the correlation search is performed through the fixed differential WFRFT-chaotic sequence $\tilde{x}_2$. As the WFRFT-CD3S signal is continuously received, the matched filter constructed by the fixed differential WFRFT-chaotic sequence $\tilde{x}_2$ is equivalent to backward correlation search. In the forward search channel, the correlation search is performed by dynamically generated differential WFRFT-chaotic sequences $\tilde{x}_{2a}$ and $\tilde{x}_{2a-1}$. Every time N chips of y_n are received, the receiver generates x_{2a} and x_{2a-1} with a total length of $2N$ chips. which is equivalent to a forward correlation search. Therefore, the two matched filters constructed by $\tilde{x}_{2a}$ and $\tilde{x}_{2a-1}$ are equivalent to forward correlation search.

In Fig. 2, $|g_{\max}|$ is the maximum magnitude of the elements in g_2, g_{2a}, and g_{2a-1}. Z_{T} is the acquisition threshold. When $|g_{\max}| > Z_{\mathrm{T}}$, the acquisition is considered to have been achieved, and the delay estimation $\hat{\tau}_0$ can be obtained from the position of $|g_{\max}|$.

Fig. 3 shows the schematic diagram of the alignment between the received signal and the local WFRFT-chaotic sequence. Since the received signal segment y_a contains $2N$ chips, y_a contains at least one complete message bit. As shown in Fig. 3, in a certain round of correlation search, the N chips in one spreading period will be all aligned.

C. DOPPLER SHIFT ESTIMATION

There are two problems with estimating the Doppler shift directly from (14). First, the unknown message bits b_k and b_{k-1} cause phase ambiguity. Second, the estimation range of the Doppler frequency shift is $|f_{\mathrm{d}}| < (2NT_{\mathrm{c}})^{-1}$. It can be seen from (11) that it is less meaningful to estimate the Doppler

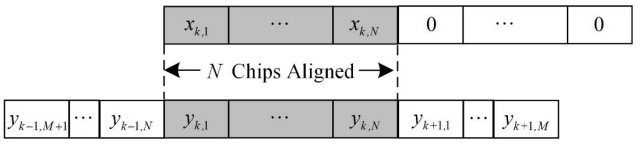

FIGURE 3. Schematic diagram of the alignment between the received signal and the local WFRFT-chaotic sequence.

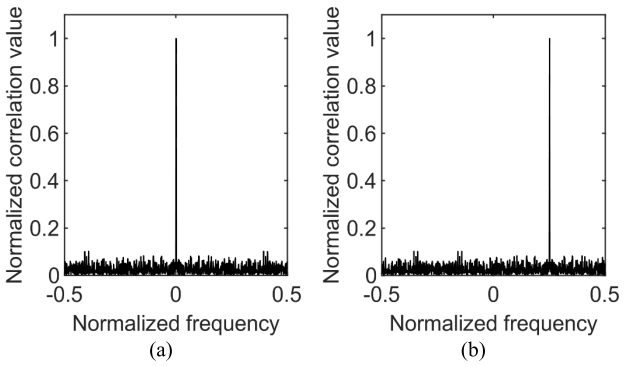

FIGURE 4. Autocorrelation function of the WFRFT-chaotic sequence in the frequency domain. (a) Doppler shift does not exist; (b) Doppler shift exists.

frequency shift in this range. In this subsection, we first make a coarse estimate of the Doppler shift to obtain a larger estimation range. Then, remove the phase ambiguity in (14) and complete the fine Doppler shift estimation.

For the DSSS system with binary PN sequence, the despread signal is a single tone signal superimposed with noise. The coarse estimate of the Doppler frequency shift can be obtained from the spectrum of the despread signal. In the WFRFT-CD3S system, since the WFRFT-chaotic sequence is a complex Gaussian distribution, the despread signal is relatively more complicated. The despread signal is given by

$$d_{k,m} = b_k x_{k,m}\bar{x}_{k,m}\exp\left(\mathrm{j}2\pi m f_{\mathrm{d}} T_{\mathrm{c}} + \mathrm{j}\phi_k\right) + v_{k,m}\bar{x}_{k,m}, \tag{23}$$

It can be seen from equation (19) that the despread signal $d_{k,m}$ is not a superposition of a single tone signal and noise. Therefore, it is not guaranteed that the Doppler frequency shift can be estimated from the spectrum of despread signal $d_{k,m}$.

The WFRFT-chaotic sequence has good autocorrelation properties in the frequency domain, as shown in Fig. 4(a). The Doppler shift of the WFRFT-chaotic sequence in the time domain results in the correlation peak shift in the frequency domain, as shown in Fig. 4(b). Therefore, in the WFRFT-CD3S system, the Doppler frequency shift can be coarsely estimated by searching the correlation peak between the received signal and the local WFRFT-CD3S sequence in the frequency domain. In this study, the correlation search in the frequency domain is implemented by a matched filter, which is given by

$$\begin{aligned} g' &= F\left[\left(F^{-1}Fy_k\right) \odot \left(\overline{F^{-1}Fx_k}\right)\right] \\ &= F\left(\bar{x}_k \odot y_k\right), \end{aligned} \tag{24}$$

where y_k contains N chips and is the synchronized received signal corresponding to x_k. Equation (24) is equivalent to analyzing the spectrum of the despread signal. Denote the m-th element in g' as g'_m, then the coarse estimate of the Doppler frequency shift can be obtained by

$$\hat{f}_{\mathrm{d1}} = \frac{1}{NT_{\mathrm{c}}}\left(\arg\max_{1\le m\le N}\left|g'_m\right|\right) - \frac{1}{NT_{\mathrm{c}}}. \tag{25}$$

Considering the periodicity of the Fourier transform of the discrete signal, the estimation range of (25) is

$$|f_{\mathrm{d}}| < \frac{1}{2T_{\mathrm{c}}}. \tag{26}$$

When the chip duration T_{c} is $1\mu s$, the estimation range of Doppler shift is (−500 kHz, 500 kHz).

The spectral resolution in (24) is $(NT_{\mathrm{c}})^{-1}$. When the Doppler frequency shift is exactly in the middle of the two frequency points, the residual Doppler frequency shift reaches the maximum. That is, the residual Doppler frequency shift is

$$|f_{\mathrm{d2}}| = \left|f_{\mathrm{d}} - \hat{f}_{\mathrm{d1}}\right| \le \frac{1}{2NT_{\mathrm{c}}}. \tag{27}$$

According to (11), the maximum attenuation caused by the residual Doppler frequency shift is 0.6366, which is still a relatively large attenuation. Therefore, it is necessary to implement fine estimation to remove the residual Doppler frequency shift.

In (12), the differential received signal $\tilde{y}_{k,m}$ contains two message bits, causing phase ambiguity. To avoid phase ambiguity caused by unknown message bits, we differentiate the chips in the synchronized received signal y_k which contains only one message bit. The Doppler frequency shift is compensated by $\hat{f}_{\mathrm{d1}}$ in the differential process. The differential received signal $\tilde{y}'_{k,m}$ is given by

$$\begin{aligned}\tilde{y}'_{k,m} &= y_{k,m+L}\mathrm{e}^{-\mathrm{j}2\pi(m+L)\hat{f}_{\mathrm{d1}}T_{\mathrm{c}}}\bar{y}_{k,m}\mathrm{e}^{\mathrm{j}2\pi m\hat{f}_{\mathrm{d1}}T_{\mathrm{c}}}\\ &= y_{k,m+L}\bar{y}_{k,m}\mathrm{e}^{-\mathrm{j}2\pi L\hat{f}_{\mathrm{d1}}T_{\mathrm{c}}},\end{aligned} \tag{28}$$

where L is the number of chips contained in the delay of differential processing.

Correspondingly, the differential WFRFT-chaotic signal $\tilde{x}'_{k,m}$ is given by

$$\tilde{x}'_{k,m} = x_{k,m+L}\bar{x}_{k,m}. \tag{29}$$

Denote the correlation value of $\tilde{y}'_{k,m}$ and $\tilde{x}'_{k,m}$ as g_{fd}. The correlation value g_{fd} is equal to

$$g_{\mathrm{fd}} = \sum_{m=1}^{N-L}\bar{\tilde{x}}'_{k,m}\tilde{y}'_{k,m}. \tag{30}$$

The expectation of g_{fd} can be calculated as

$$\begin{aligned}\mu_{g_{\mathrm{fd}}} &= \mathrm{E}\left(g_{\mathrm{fd}}\right)\\ &= \mathrm{E}\left(\sum_{m=1}^{N-L}\bar{\tilde{x}}'_{k,m}\tilde{y}'_{k,m}\right)\\ &= \mathrm{E}\left(\sum_{m=1}^{N-L}\bar{x}_{k,m+N/2}x_{k,m}y_{k,m+N/2}\bar{y}_{k,m}\mathrm{e}^{-\mathrm{j}\pi N\hat{f}_{\mathrm{d1}}T_{\mathrm{c}}}\right)\\ &= (N-L)\,P_{\mathrm{c}}^2\mathrm{e}^{\mathrm{j}2\pi L\left(f_{\mathrm{d}}-\hat{f}_{\mathrm{d1}}\right)T_{\mathrm{c}}}.\end{aligned} \tag{31}$$

The fine estimation of the Doppler frequency shift can be calculated by

$$\hat{f}_{\mathrm{d2}} = \frac{\theta}{2\pi LT_{\mathrm{c}}}, \tag{32}$$

where the phase angle θ is given by

$$\theta = \arg\left(g_{\mathrm{fd}}\right). \tag{33}$$

Since L is less than N, it can be seen from (27) that the phase angle in (33) is in $(-\pi, \pi)$. That is, residual Doppler frequency shift f_{d2} is small enough to not cause phase ambiguity.

In summary, the estimated value of the Doppler shift is

$$\hat{f}_{\mathrm{d}} = \hat{f}_{\mathrm{d1}} + \hat{f}_{\mathrm{d2}}. \tag{34}$$

IV. THEORETICAL ANALYSIS OF PERFORMANCE

A. FALSE ALARM PROBABILITY

The false alarm occurs when the received signal is misaligned with the local WFRFT-chaotic sequence but the magnitude of the correlation value is greater than the acquisition threshold. For ease of writing, we assume that the delay between the received signal and the local WFRFT-chaotic sequence is N chips. This assumption does not affect the theoretical analysis results. Then the correlation value when the received signal and the local WFRFT-chaotic sequence are not aligned is given by

$$g_{\mathrm{u}} = \sum_{m=1}^{N}\bar{x}_{k,m}x_{k-1,m}y_{k-1,m}\bar{y}_{k-2,m}. \tag{35}$$

The signal-to-noise ratio (SNR) is defined as

$$S_{\mathrm{NR}} = \frac{P_{\mathrm{c}}}{\sigma^2}. \tag{36}$$

The correlation value g_{u} obeys a complex Gaussian distribution according to the central limit theorem. The mathematical expectation of g_{u} can be derived as

$$\begin{aligned}u_{g_{\mathrm{u}}} &= \mathrm{E}\left(\sum_{m=1}^{N}\bar{x}_{k,m}x_{k-1,m}y_{k-1,m}\bar{y}_{k-2,m}\right)\\ &= \mathrm{E}\Bigg[\sum_{m=1}^{N}\bar{x}_{k,m}x_{k-1,m}\\ &\quad\times\left(b_{k-1}x_{k-1,m}\mathrm{e}^{\mathrm{j}2\pi mf_{\mathrm{d}}T_{\mathrm{c}}+\mathrm{j}\phi_{k-1}} + v_{k-1,m}\right)\\ &\quad\cdot\left(b_{k-2}\bar{x}_{k-2,m}\mathrm{e}^{-\mathrm{j}2\pi mf_{\mathrm{d}}T_{\mathrm{c}}-\mathrm{j}\phi_{k-2}} + \bar{v}_{k-2,m}\right)\Bigg] = 0.\end{aligned} \tag{37}$$

The variance of g_{u} can be derived as

$$\sigma_{g_{\mathrm{u}}}^2 = \mathrm{E}\left(\bar{g}_{\mathrm{u}}g_{\mathrm{u}}\right) - \mathrm{E}\left(\bar{g}_{\mathrm{u}}\right)\mathrm{E}\left(g_{\mathrm{u}}\right)$$

$$
\begin{aligned}
&= \mathrm{E}\left\{\left[\sum_{m=1}^{N} x_{k,m}\bar{x}_{k-1,m}\right.\right. \\
&\quad \times \left(b_{k-1}\bar{x}_{k-1,m}\mathrm{e}^{-\mathrm{j}2\pi mf_{\mathrm{d}}T_{\mathrm{c}}-\mathrm{j}\phi_{k-1}} + \bar{v}_{k-1,m}\right) \\
&\quad \left.\cdot \left(b_{k-2}x_{k-2,m}\mathrm{e}^{\mathrm{j}2\pi mf_{\mathrm{d}}T_{\mathrm{c}}+\mathrm{j}\phi_{k-2}} + v_{k-2,m}\right)\right] \\
&\quad \cdot \left[\sum_{m=1}^{N} \bar{x}_{k,m}x_{k-1,m}\left(b_{k-1}x_{k-1,m}\mathrm{e}^{\mathrm{j}2\pi mf_{\mathrm{d}}T_{\mathrm{c}}+\mathrm{j}\phi_{k-1}}\right.\right. \\
&\quad \left.\left. + v_{k-1,m}\right)\cdot \left(b_{k-2}\bar{x}_{k-2,m}\mathrm{e}^{-\mathrm{j}2\pi mf_{\mathrm{d}}T_{\mathrm{c}}-\mathrm{j}\phi_{k-2}} + \bar{v}_{k-2,m}\right)\right]\Bigg\} \\
&= \mathrm{E}\left[\sum_{m=1}^{N} x_{k,m}\bar{x}_{k,m}\bar{x}_{k-1,m}x_{k-1,m}\right. \\
&\quad \times \left(\bar{x}_{k-1,m}x_{k-1,m}x_{k-2,m}\bar{x}_{k-2,m}\right. \\
&\quad + \bar{x}_{k-1,m}x_{k-1,m}v_{k-2,m}\bar{v}_{k-2,m} \\
&\quad + \bar{v}_{k-1,m}\bar{v}_{k-1,m}x_{k-2,m}\bar{x}_{k-2,m} \\
&\quad \left.\left. + \bar{v}_{k-1,m}\bar{v}_{k-1,m}v_{k-2,m}\bar{v}_{k-2,m}\right)\right] \\
&= NP_{\mathrm{c}}^2\left(P_{\mathrm{c}}^2 + P_{\mathrm{c}}\sigma^2 + P_{\mathrm{c}}\sigma^2 + \sigma^4\right) \\
&= NP_{\mathrm{c}}^4\left(1+\frac{1}{S_{\mathrm{NR}}}\right)^2. \qquad (38)
\end{aligned}
$$

Denote the magnitude of g_{u} as η_{u}. Since the mathematical expectation of g_{u} is 0, and the real and imaginary parts of g_{u} are independent and identically distributed, η_{u} obeys the Rayleigh distribution. The probability density function of η_{u} can be expressed as

$$
f_{\eta_{\mathrm{u}}}(\eta_{\mathrm{u}}) = \frac{2\eta_{\mathrm{u}}}{\sigma_{g_{\mathrm{u}}}^2}\exp\left(-\frac{\eta_{\mathrm{u}}^2}{\sigma_{g_{\mathrm{u}}}^2}\right). \qquad (39)
$$

The false alarm probability of time acquisition can be derived as

$$
\begin{aligned}
P_{\mathrm{F}} &= P\{\eta_{\mathrm{u}} \geq Z_{\mathrm{T}}\} \\
&= \int_{Z_{\mathrm{T}}}^{\infty} f_{\eta_{\mathrm{u}}}(\eta_{\mathrm{u}})\mathrm{d}\eta_{\mathrm{u}} \\
&= \exp\left(-\frac{Z_{\mathrm{T}}^2}{\sigma_{g_{\mathrm{u}}}^2}\right) \\
&= \exp\left[-\frac{Z_{\mathrm{T}}^2}{NP_{\mathrm{c}}^4}\left(1+\frac{1}{S_{\mathrm{NR}}}\right)^{-2}\right]. \qquad (40)
\end{aligned}
$$

B. DETECTION PROBABILITY

Detection occurs when the received signal is aligned with the local WFRFT-chaotic sequence and the magnitude of the correlation value is greater than the acquisition threshold. The correlation value when the received signal is aligned with the local WFRFT-chaotic sequence is given by

$$
g_{\mathrm{s}} = \sum_{m=1}^{N} \bar{x}_{k,m}x_{k-1,m}y_{k,m}\bar{y}_{k-1,m}. \qquad (41)
$$

The correlation value g_{s} obeys a complex Gaussian distribution according to the central limit theorem. According to (14), the mathematical expectation of g_{s} is equal to

$$
\begin{aligned}
\mu_{g_{\mathrm{s}}} &= \mathrm{E}\left(\sum_{m=1}^{N} \bar{x}_{k,m}x_{k-1,m}y_{k,m}\bar{y}_{k-1,m}\right) \\
&= NP_{\mathrm{c}}^2 b_k b_{k-1}\mathrm{e}^{\mathrm{j}2\pi Nf_{\mathrm{d}}T_{\mathrm{c}}}. \qquad (42)
\end{aligned}
$$

The variance of g_{s} can be derived as

$$
\begin{aligned}
\sigma_{g_{\mathrm{s}}}^2 &= \mathrm{E}(\bar{g}_{\mathrm{s}}g_{\mathrm{s}}) - \mathrm{E}(\bar{g}_{\mathrm{s}})\,\mathrm{E}(g_{\mathrm{s}}) \\
&= \mathrm{E}\left[\left(\sum_{m=1}^{N} x_{k,m}\bar{x}_{k-1,m}\bar{y}_{k,m}y_{k-1,m}\right)\right. \\
&\quad \left.\cdot \left(\sum_{m=1}^{N} \bar{x}_{k,m}x_{k-1,m}y_{k,m}\bar{y}_{k-1,m}\right)\right] - N^2P_{\mathrm{c}}^4 \\
&= \mathrm{E}\left\{\left[\sum_{m=1}^{N} x_{k,m}\bar{x}_{k-1,m}\left(b_k\bar{x}_{k,m}\mathrm{e}^{-\mathrm{j}2\pi mf_{\mathrm{d}}T_{\mathrm{c}}-\mathrm{j}\phi_k} + \bar{v}_{k,m}\right)\right.\right. \\
&\quad \cdot \left(b_{k-1}x_{k-1,m}\mathrm{e}^{\mathrm{j}2\pi mf_{\mathrm{d}}T_{\mathrm{c}}+\mathrm{j}\phi_{k-1}} + v_{k-1,m}\right)\Bigg] \\
&\quad \cdot \left[\sum_{m=1}^{N} \bar{x}_{k,m}x_{k-1,m}\left(b_kx_{k,m}\mathrm{e}^{\mathrm{j}2\pi mf_{\mathrm{d}}T_{\mathrm{c}}+\mathrm{j}\phi_k} + v_{k,m}\right)\right. \\
&\quad \left.\left.\left.\cdot \left(b_{k-1}\bar{x}_{k-1,m}\mathrm{e}^{-\mathrm{j}2\pi mf_{\mathrm{d}}T_{\mathrm{c}}-\mathrm{j}\phi_{k-1}} + \bar{v}_{k-1,m}\right)\right]\right\} - N^2P_{\mathrm{c}}^4 \\
&= \mathrm{E}\left[\sum_{m=1}^{N} x_{k,m}\bar{x}_{k,m}\bar{x}_{k-1,m}x_{k-1,m}\left(\bar{x}_{k,m}x_{k,m}v_{k-1,m}\bar{v}_{k-1,m}\right.\right. \\
&\quad + \bar{v}_{k,m}\bar{v}_{k,m}x_{k-1,m}\bar{x}_{k-1,m} + \bar{v}_{k,m}\bar{v}_{k,m}v_{k-1,m}\bar{v}_{k-1,m} \\
&\quad \left.\left. + \sum_{m=1}^{N} \bar{x}_{k,m}x_{k,m}x_{k-1,m}\bar{x}_{k-1,m}\right)\right] - N^2P_{\mathrm{c}}^4 \\
&= NP_{\mathrm{c}}^2\left(P_{\mathrm{c}}\sigma^2 + P_{\mathrm{c}}\sigma^2 + \sigma^4 + NP_{\mathrm{c}}^2\right) - N^2P_{\mathrm{c}}^4 \\
&= NP_{\mathrm{c}}^4\left(\frac{2}{S_{\mathrm{NR}}} + \frac{1}{S_{\mathrm{NR}}^2}\right). \qquad (43)
\end{aligned}
$$

Denote the magnitude of g_{s} as η_{s} and the magnitude of $\mu_{g_{\mathrm{s}}}$ as $\mu_{\eta_{\mathrm{s}}}$. Since the WFRFT-chaotic sequence x_k is a complex Gaussian distribution, the real and imaginary parts of g_{s} are correlated when $S_{\mathrm{NR}} = +\infty$. As the SNR decreases, the correlation between the real and imaginary parts of g_{s} decreases. When the SNR is low, η_{s} approximately obeys the Rice distribution. The probability density function of η_{s} can be expressed as

$$
f_{\eta_{\mathrm{s}}}(\eta_{\mathrm{s}}) \approx \frac{2\eta_{\mathrm{s}}}{\sigma_{g_{\mathrm{s}}}^2}\exp\left(-\frac{\eta_{\mathrm{s}}^2+\mu_{\eta_{\mathrm{s}}}^2}{\sigma_{g_{\mathrm{s}}}^2}\right)I_0\left(\frac{2\eta_{\mathrm{s}}\mu_{\eta_{\mathrm{s}}}}{\sigma_{g_{\mathrm{s}}}^2}\right), \qquad (44)
$$

where $I_0(\cdot)$ is the zeroth-order modified Bessel function, one of the definition equations of which being

$$I_0(x) = \frac{1}{2\pi}\int_0^{2\pi} \exp(x\cos\theta)\,\mathrm{d}\theta. \tag{45}$$

The detection probability of time acquisition can be derived as [22]

$$\begin{aligned} P_{\mathrm{D}} &= P\{\eta_{\mathrm{s}} \geq Z_{\mathrm{T}}\} \\ &= \int_{Z_{\mathrm{T}}}^{\infty} f_{\eta_{\mathrm{s}}}(\eta_{\mathrm{s}})\mathrm{d}\eta_{\mathrm{s}} \\ &= \int_{Z_{\mathrm{T}}}^{\infty} f \frac{2\eta_{\mathrm{s}}}{\sigma_{g_{\mathrm{s}}}^2}\exp\left(-\frac{\eta_{\mathrm{s}}^2+\mu_{\eta_{\mathrm{s}}}^2}{\sigma_{g_{\mathrm{s}}}^2}\right) I_0\left(\frac{2\eta_{\mathrm{s}}\mu_{\eta_{\mathrm{s}}}}{\sigma_{g_{\mathrm{s}}}^2}\right)\mathrm{d}\eta_{\mathrm{s}} \\ &= Q\left(\frac{\sqrt{2}\mu_{\eta_{\mathrm{s}}}}{\sigma_{g_{\mathrm{s}}}}, \frac{\sqrt{2}\,Z_{\mathrm{T}}}{\sigma_{g_{\mathrm{s}}}}\right), \end{aligned} \tag{46}$$

where the Marcum Q-function is defined as [23]

$$Q(a,b) = \int_b^{\infty} x\exp\left(-\frac{a^2+x^2}{2}\right) I_0(ax)\,\mathrm{d}x. \tag{47}$$

C. ROOT MEAN SQUARE ERROR OF DOPPLER SHIFT ESTIMATION

The residual frequency shift of the coarse Doppler frequency shift estimation is processed by the fine estimation. Therefore, the RMSE of the Doppler frequency shift estimation is determined by the fine estimation.

According to (43), the variance of g_{fd} can be easily derived as

$$\sigma_{g_{\mathrm{fd}}}^2 = (N-L)P_{\mathrm{c}}^4\left(\frac{2}{S_{\mathrm{NR}}} + \frac{1}{S_{\mathrm{NR}}^2}\right). \tag{48}$$

Similar to g_{s}, it can be known that the phase angle of g_{fd} follows the Rice phase distribution. The probability density function of phase angle θ can be expressed as [24]

$$\begin{aligned} f_\theta(\theta) = &\frac{1}{2\pi}\exp(-K) + \frac{1}{2}\sqrt{\frac{K}{\pi}}\cos\theta \\ &\cdot\exp\left(-K\sin^2\theta\right)\left[1+\mathrm{erf}\left(\sqrt{K}\cos\theta\right)\right], \end{aligned} \tag{49}$$

where $\mathrm{erf}(x) = \frac{2}{\sqrt{\pi}}\int_0^x \exp\left(-u^2\right)\mathrm{d}u$ is the error function,

$$K = \frac{\left|\mu_{g_{\mathrm{fd}}}\right|^2}{\sigma_{g_{\mathrm{fd}}}^2} = (N-L)\frac{S_{\mathrm{NR}}^2}{2S_{\mathrm{NR}}+1}. \tag{50}$$

According to [26], the variance of the phase angle θ is approximately equal to

$$\sigma_\theta^2 \approx \frac{1}{2K} = \frac{2S_{\mathrm{NR}}+1}{2(N-L)S_{\mathrm{NR}}^2}. \tag{51}$$

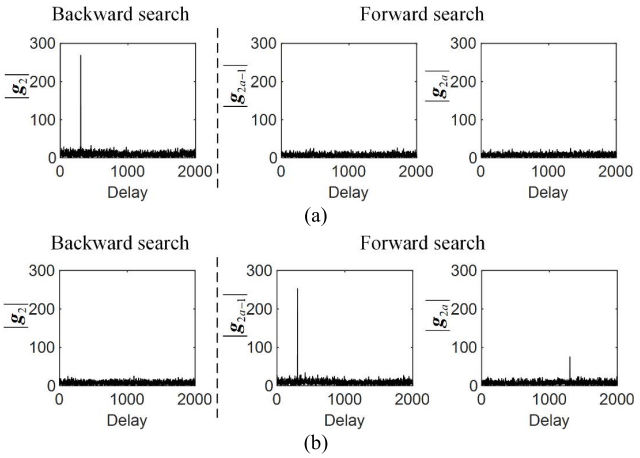

FIGURE 5. Output of the matched filters when time acquisition happens. (a) The received signal lags the local WFRFT-chaotic sequence. (b) The received signal leads the local WFRFT-chaotic sequence.

The estimate obtained by (32) is unbiased. Combining (32) and (51), the RMSE of the Doppler shift estimate is approximately equal to

$$\begin{aligned} \varepsilon(L) &= \sqrt{\frac{\sigma_\theta^2}{(2\pi L T_{\mathrm{c}})^2}} \\ &\approx \sqrt{\frac{2S_{\mathrm{NR}}+1}{8\pi^2(N-L)L^2T_{\mathrm{c}}^2S_{\mathrm{NR}}^2}}. \end{aligned} \tag{52}$$

According to (52), $\varepsilon(L)$ takes the minimum value when

$$L = \frac{2}{3}N. \tag{53}$$

V. SIMULATION ANALYSIS

In all simulations, the system initial value $c_{0,1}$, the Tent mapping parameters q, the WFRFT order α, the spreading factor N and the chip duration T_{c} are set to 0.3, 0.65, 0.94, 1000 and $1\mu s$, respectively.

A. SIMULATION ANALYSIS OF TIME ACQUISITION

Fig. 5 shows the output of the matched filters when time acquisition happens. The Doppler frequency shift is set to 5 kHz and the SNR is set to 10 dB in Fig. 5. The correlation peak attenuation caused by Doppler frequency shift is avoided by differencing. When the received signal lags the local WFRFT-chaotic sequence, the correlation peak appears in the backward search channel. When the received signal leads the local WFRFT-chaotic sequence, the correlation peak appears in the forward search channel. In Fig. 5(b), the attenuated correlation peak appearing in g_{2a} is not caused by Doppler frequency shift but is caused by partial chips alignment between the received signal and the local WFRFT-chaotic sequence. Fig. 5 shows that the proposed bidirectional correlation search method can acquire the aperiodic WFRFT-CD3S signal with Doppler frequency shift.

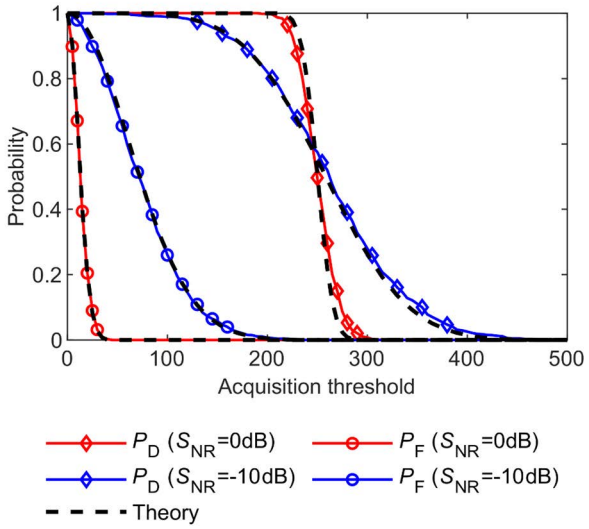

FIGURE 6. False alarm probability and detection probability based on the acquisition threshold.

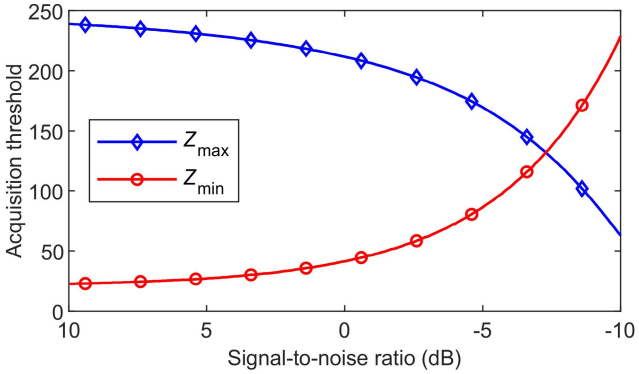

FIGURE 7. Superior limit and inferior limit of the acquisition threshold based on the SNR.

Fig. 6 shows the curves of false alarm probability and detection probability as a function of the acquisition threshold. It can be seen from Fig. 6 that the theoretical results of detection probability and false alarm probability are basically consistent with the simulation results. For the detection probability when the SNR is 0 dB, there is a deviation between the theoretical value and the simulated value but the deviation is limited. Both the detection probability and the false alarm probability show an overall decreasing trend with the increase of the acquisition threshold. Assume that the system detection probability index P_{FI} is set to 0.001. When $S_{NR} = 0$dB, there is an acquisition threshold $Z_T \in [41, 211]$ such that $P_F \leq P_{FI}$ and $P_D \geq P_{DI}$. When $S_{NR} = -10$dB there is no acquisition threshold Z_T that P_{DI} and P_{FI} can be satisfied at the same time.

It can be inferred from Fig. 6 that there is an optimal acquisition threshold Z_T^* such that P_{DI} and P_{FI} can be satisfied at the lowest SNR. To analyze the optimal acquisition threshold Z_T^* of the proposed bidirectional correlation search method, Fig. 7 shows the curves of the acquisition threshold superior limit Z_{max} and inferior limit Z_{min} as a function of SNR.

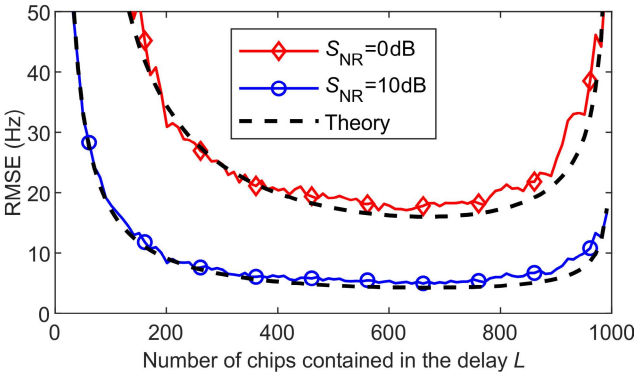

FIGURE 8. RMSE of the doppler frequency shift estimation based on the number of chips contained in the delay.

In Fig. 7. P_{DI} and P_{FI} are set to 0.999 and 0.001, respectively. The acquisition threshold superior limit Z_{max} is the highest acquisition threshold at which P_{DI} can be satisfied. The acquisition threshold inferior limit Z_{min} is the lowest acquisition threshold at which P_{FI} can be satisfied. When SNR is greater than -7.3dB, Z_{min} is lower than Z_{max}. When SNR is equal to -7.3 dB, Z_{min} and Z_{max} are equal to 131.8. This means that when SNR is greater than -7.3dB, setting Z_T to 131.8 can make P_{DI} and P_{FI} be satisfied at the same time. When SNR is lower than -7.3dB, Z_{min} is greater than Z_{max}. Therefore, P_{DI} and P_{FI} cannot be satisfied at the same time when SNR is lower than -7.3 dB. In summary, the optimal acquisition threshold Z_T^* is 131.8 and the minimum acquirable SNR is -7.3dB under the given simulation conditions.

B. SIMULATION ANALYSIS OF DOPPLER SHIFT ESTIMATION

To analyze the influence of the delay in the difference process on the Doppler frequency estimation error, Fig. 8 shows the RMSE of the Doppler frequency estimation based on the number of chips contained in the delay. As the SNR decreases and the number of chips L increases, the deviation between the theoretical and simulated results increases. The reason is that as the SNR decreases and L increases, the value of K in (50) decreases, thereby increasing the approximation error in (51). The deviation between the theoretical and simulated results in Fig. 8 is limited, which means that it is still feasible to design the system parameters according to the theoretical results in engineering. To ensure the resolution when the RMSE is small, the vertical axis of Fig. 8 is limited to [0 Hz, 50 Hz] and the simulation results when L is close to N or 0 are not shown in Fig. 8. When L is close to N or 0, the RMSE rises rapidly, and L is not suitable to be taken near N or 0. Equation (53) shows that the RMSE is minimized under the given simulation conditions when $L = 2N/3 \approx 667$. However, Fig. 8 shows that the RMSEs are close to each other when $L \in [550, 750]$. Therefore, L can take a value around $2N/3$ in engineering.

Fig. 9 shows the RMSE of the Doppler shift estimation as a function of SNR for different residual Doppler shifts. The

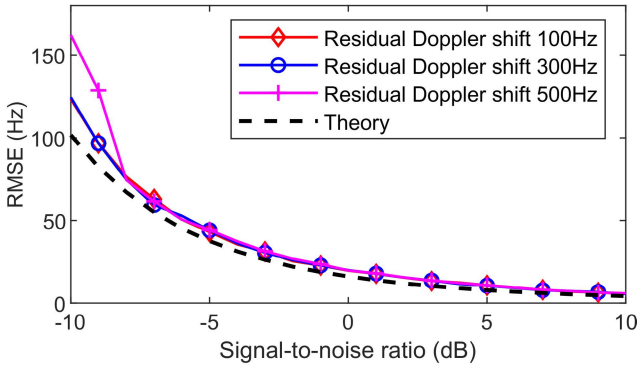

FIGURE 9. RMSE of the doppler frequency shift estimation based on SNR.

delay between the differentiated chips is set to $L = 667$. The residual Doppler shift is in $[-500\text{Hz}, 500\text{Hz}]$ under the given simulation condition. Therefore, the residual Doppler shifts in Fig. 9 are set to 100 Hz, 300 Hz, and 500 Hz. The RMSEs under different residual Doppler frequency shifts are close to each other when $S_{\text{NR}} \geq -8$ dB. When $S_{\text{NR}} < -8$dB and the residual Doppler shift is 500 Hz, the RMSE of Doppler shift estimation increases significantly. The reason for this phenomenon is the phase ambiguity caused by the residual Doppler shift superimposed noise. It can be inferred from Fig. 9 that the residual Doppler shift does not affect the estimation error in the absence of phase ambiguity. However, in (33), higher residual Doppler shifts are more likely to cause phase ambiguity under the influence of noise. The minimum acquirable SNR in the time acquisition phase is -7.3dB. When $S_{\text{NR}} > -7.3$dB, the RMSE of Doppler shift estimation is less than 63 Hz.

VI. CONCLUSION

In this paper, we acquire the aperiodic WFRFT-CD3S signal with Doppler shift through two steps of time acquisition and Doppler shift estimation. The false alarm probability and detection probability of time acquisition, and the RMSE of Doppler frequency shift estimation are theoretically analyzed. The theoretical results are verified by simulation results. The simulation results show that the proposed bidirectional correlation search method can achieve acquisition regardless of whether the received WFRFT-CD3S signal leads or lags behind the local WFRFT-chaotic sequence. The optimal acquisition threshold is obtained through simulation analysis. The optimal acquisition threshold is 131.8 and the minimum acquirable SNR is -7.3 dB under the simulation conditions given in Section V. When the SNR is greater than -7.3 dB, the detection probability is greater than 0.999, the false alarm probability is less than 0.001, and the RMSE of Doppler frequency shift estimation is less than 63 Hz. The Doppler frequency shift is assumed to be constant in this study but the proposed method is applicable to the data link of UAV where the Doppler frequency varies.

The optimal acquisition threshold was obtained by numerical simulation and was not derived theoretically in this study. In engineering, the optimal capture threshold can also be obtained through the numerical analysis method in Section V-A. It will be our future work to reduce the minimum acquirable SNR and derive a theoretical solution for the optimal acquisition threshold.

REFERENCES

[1] G. Kaddoum, "Wireless chaos-based communication systems: A comprehensive survey," *IEEE Access*, vol. 4, pp. 2621–2648, 2016.
[2] B. Shen and J. Wang, "Chip rate and pseudo-noise sequence estimation for direct sequence spread spectrum signals," *IET Signal Process.*, vol. 11, no. 6, pp. 727–733, Aug. 2017.
[3] L. Novosel, G. Šišul, Ž. Ilić, and J. Božek, "Performance enhancement of LR WPAN spread spectrum system using chaotic spreading sequences," *AEU-Int. J. Electron. Commun.*, vol. 118, May 2020, Art. no. 153131.
[4] M. Eisencraft, L. H. A. Monteiro, and D. C. Soriano, "White Gaussian chaos," *IEEE Commun. Lett.*, vol. 21, no. 8, pp. 1719–1722, Aug. 2017.
[5] G. Yuan, Z. Chen, X. Gao, and Y. Zhang, "Enhancing the security of chaotic direct sequence spread spectrum communication through WFRFT," *IEEE Commun. Lett.*, vol. 25, no. 9, pp. 2834–2838, Sep. 2021.
[6] X. Wang, L. Mei, Z. Wang, and N. Zhang, "On the probability density function of the real and imaginary parts in WFRFT signals," *China Commun.*, vol. 13, no. 9, pp. 44–52, Sep. 2016.
[7] W. Wang, Y. Tong, L. Li, A.-A. Lu, L. You, and X. Gao, "Near optimal timing and frequency offset estimation for 5G integrated LEO satellite communication system," *IEEE Access*, vol. 7, pp. 113298–113310, 2019.
[8] Q. Zhang, H. Sun, Z. Feng, H. Gao, and W. Li, "Data-aided Doppler frequency shift estimation and compensation for UAVs," *IEEE Internet Things J.*, vol. 7, no. 1, pp. 400–415, Jan. 2020.
[9] Y. Shen and Y. Xu, "Analysis of the code phase migration and Doppler frequency migration effects in the coherent integration of direct-sequence spread-spectrum signals," *IEEE Access*, vol. 7, pp. 26581–26594, 2019.
[10] H. Zhao, Y. Chen, W. Feng, and C. Zhuang, "A dual-channel acquisition method based on extended replica folding algorithm for long pseudo-noise code in inter-satellite links," *Sensors*, vol. 18, no. 6, p. 1717, May 2018.
[11] Y. Pan, T. Zhang, G. Zhang, and Z. Luo, "A novel acquisition algorithm based on PMF-apFFT for BOC modulated signals," *IEEE Access*, vol. 7, pp. 46686–46694, 2019.
[12] F. Zhou, L. Zhao, L. Li, Y. Hu, X. Jiang, J. Yu, and G. Liang, "GNSS signal acquisition algorithm based on two-stage compression of code-frequency domain," *Appl. Sci.*, vol. 12, no. 12, p. 6255, Jun. 2022.
[13] Z. Deng, B. Jia, S. Tang, X. Fu, and J. Mo, "Fine frequency acquisition scheme in weak signal environment for a communication and navigation fusion system," *Electronics*, vol. 8, no. 8, p. 829, Jul. 2019.
[14] F. Gao and H. Xia, "Fast GNSS signal acquisition with Doppler frequency estimation algorithm," *GPS Solutions*, vol. 22, no. 4, p. 103, Oct. 2018.
[15] S. Liu, T. Shan, R. Tao, Y. Zhang, G. Zhang, F. Zhang, and Y. Wang, "Sparse discrete fractional Fourier transform and its applications," *IEEE Trans. Signal Process.*, vol. 62, no. 24, pp. 6582–6595, Dec. 2014.
[16] H. Zhang, T. Shan, S. Liu, and R. Tao, "Optimized sparse fractional Fourier transform: Principle and performance analysis," *Signal Process.*, vol. 174, Sep. 2020, Art. no. 107646.
[17] G. Yuan, Z. Chen, X. Gao, J. He, and H. Jia, "A synchronization approach based on bidirectional correlation search for aperiodic chaotic direct sequence spread spectrum signals," *IEEE Access*, vol. 8, pp. 190390–190402, 2020.
[18] N. Akbar, S. Yan, A. M. Khattak, and N. Yang, "On the pilot contamination attack in multi-cell multiuser massive MIMO networks," *IEEE Trans. Commun.*, vol. 68, no. 4, pp. 2264–2276, Apr. 2020.
[19] W. Xu, C. Yuan, S. Xu, H. Q. Ngo, and W. Xiang, "On pilot spoofing attack in massive MIMO systems: Detection and countermeasure," *IEEE Trans. Inf. Forensics Security*, vol. 16, pp. 1396–1409, 2021.
[20] F. Wang, X. Chen, A. Men, L. Zhang, and S. Wu, "Carrier frequency offset estimation for FM and symbiotic FM radio data system hybrid signal," *China Commun.*, vol. 17, no. 1, pp. 129–139, Jan. 2020.
[21] X. Fang, X. Sha, and L. Mei, "Guaranteeing wireless communication secrecy via a WFRFT-based cooperative system," *China Commun.*, vol. 12, no. 9, pp. 76–82, Sep. 2015.

[22] N. C. Beaulieu and K. T. Hemachandra, "Novel representations for the bivariate rician distribution," *IEEE Trans. Commun.*, vol. 59, no. 11, pp. 2951–2954, Nov. 2011.
[23] A. Gil, J. Segura, and N. M. Temme, "The asymptotic and numerical inversion of the Marcum Q-function," *Stud. Appl. Math.*, vol. 133, no. 2, pp. 257–278, 2014.
[24] Z. Luo, Y. Zhan, and E. Jonckheere, "Analysis on functions and characteristics of the Rician phase distribution," in *Proc. IEEE/CIC Int. Conf. Commun. China (ICCC)*, Chongqing, China, Aug. 2020, pp. 306–311.

JIANGYAN HE received the B.S. and M.S. degrees in mathematic from Hebei Normal University, Shijiazhuang, China, in 2005 and 2008, respectively. She is currently a Lecturer with the Shijiazhuang Campus of AEU, Shijiazhuang. Her research interests include the areas of the basic theory of nonlinear functional analysis and anti-jamming communication.

GUOGANG YUAN was born in Sichuan, China, in 1994. He received the B.S. degree in unmanned aerial vehicle engineering from the Mechanical Engineering College, Shijiazhuang, China, in 2016, and the M.S. degree in control science and engineering from the Shijiazhuang Campus of AEU, Shijiazhuang, in 2018, where he is currently pursuing the Ph.D. degree in control science and engineering. His research interests include the areas of chaotic communication and physical layer security.

ZILI CHEN was born in Shanxi, China, in 1964. He received the B.S. degree from the Mechanical Engineering College, Shijiazhuang, China, in 1984, and the M.S. degree from the Nanjing University of Science and Technology, Nanjing, China, in 1987. He is currently a Full Professor with the Shijiazhuang Campus of AEU, Shijiazhuang. His research interests include the areas of UAV-assisted communication and signal processing.

XIJUN GAO received the B.S. degree in electronic information engineering from Dalian Maritime University, China, in 2009, and the M.S. degree in communication and information system and the Ph.D. degree in control science and engineering from the Mechanical Engineering College, Shijiazhuang, China, in 2011 and 2015, respectively. He is currently pursuing the degree in UAV communication technology.